Enhanced Gas Recovery with CO_2 Sequestration: the Effect of Medium Heterogeneity on the Dispersion of Supercritical CO_2-CH_4

Abdolvahab Honari[1], Branko Bijeljic[2], Michael L. Johns[1], Eric F. May[1,*]

[1] Centre for Energy, School of Mechanical and Chemical Engineering M050, University of Western Australia, 35 Stirling Highway, Crawley 6009, Western Australia, Australia.

[2] Department of Earth Science and Engineering, Imperial College London, Prince Consort Road, London SW7 2BP, United Kingdom.

* Corresponding author: Fax.: +61 8 6488 1024, Tel.: +61 8 6488 2954,

Email address Eric.May@uwa.edu.au

Abstract

Reinjection of CO_2 into producing natural gas reservoirs is considered as a promising technology to improve gas recovery, mitigate atmospheric emissions and control climate change. However, natural gas and CO_2 are miscible at reservoir conditions and could result in CO_2 contamination of produced natural gas. This mixing process and consequently the viability of Enhanced Gas Recovery (EGR) projects can be quantitatively determined by reservoir simulations – such simulations require a description of gas dispersion. Here we conduct fluid transport experiments through carbonate and sandstone rock cores at various reservoir conditions to evaluate the effect of medium heterogeneity on the dispersion between supercritical CO_2 and CH_4, accounting for erroneous contributions from entrance/exit and gravitational effects. Early breakthrough and long-tailed profiles are observed for one of the carbonate cores (Ketton) which is attributed to the existence of intra-grain micro-pores, which results in a persistent pre-asymptotic transport regime. Thus a revised model (Mobile-Immobile Model) was successfully used for this core to obtain dispersion coefficients characteristic of the eventual asymptotic regime. Both heterogeneous carbonate rocks considered exhibit higher dispersion than that observed in previously-measured homogeneous sandstone cores (Honari et al., 2013). The power law describing the dependency of dispersion coefficient on Péclet number at comparatively high interstitial displacement velocities gave an exponent of 1.2 for sandstones and 1.4 for carbonates, consistent with literature predictions (Bijeljic and Blunt, 2006; Bijeljic et al., 2011) based on pore-scale simulations.

Keywords: Enhanced gas recovery, Carbon dioxide, Sequestration, Dispersion, Heterogeneous porous media, Carbonates.

1. Introduction

Carbonate formations contain more than half of the world's current oil reserves together with a huge portion of the proved gas resources in the Middle East (Ahlbrandt et al., 2005; Akbar et al., 2000; Roehl and Choquette, 1985). They are naturally fractured and their porosity and permeability are heterogeneously distributed, with the fracture matrix having a wide range of pore sizes that lead to complex flow and transport processes behavior. Extensive efforts have been made for decades to improve oil recovery from such reservoirs using various approaches including chemical, gas injection and thermal methods. Alvarado and Manrique (2010) reviewed more than 1500 enhanced oil recovery (EOR) projects worldwide and reported that 18% of the total projects were implemented in carbonate reservoirs. Among all EOR methods, gas flooding (especially CO_2 flooding) has recently become arguably the most attractive approach for carbonate formations due to the potential for greenhouse gas mitigation. In the USA, nearly 85% of EOR projects in carbonate reservoirs involve CO_2 flooding (Manrique et al., 2007).

Even though EOR via CO_2 flooding is a well-established method to improve the recovery factor of oil reservoirs and geologically sequester CO_2, enhanced gas recovery (EGR) with CO_2 flooding/sequestration has not been widely considered by the oil and gas industry. This process not only can safely store CO_2 within the formation but also can improve the natural gas recovery by upholding the reservoir pressure and enhancing sweep efficiency and production rates. However, natural gas and CO_2 are entirely miscible in all proportions and consequently the risks of mixing these fluids within the reservoir formation and early CO_2 breakthrough into production wells are the main hurdles for EGR implementation. These associated risks and uncertainties of EGR projects can be estimated by using reservoir simulations in which fluid flow in reservoir formations can be quantitatively modeled and, in principle, the mixing process between the injected CO_2 and natural gas captured. Doing so reliably, however, requires (1) adequate characterization of physical dispersion at all relevant length-scales, and (2) that numerical dispersion in such simulations be kept sufficiently small. The latter remains an ongoing challenge in practice (e.g. Adepoju et al., 2013; Peaceman, 1977). Extensive studies of dispersion at the field scale have been published (Arya et al., 1988; Coats et al., 2009; Lake, 1989) but generalizing the results of these studies is not straightforward. Physical dispersion at smaller length scales is also important because, as discussed below, the description of transport at the core scale can play an important role in the prediction of mixing at the field scale, particularly for carbonate formations. These

challenges to describing the mixing of CO_2 and natural gas have limited EGR projects to only a few field trials (Pooladi-Darvish et al., 2008; Vandeweijer et al., 2011). The only current field-scale EGR project is the Rotliegend K12-B gas reservoir, located offshore of the Netherlands, which started in 2004 after 17 years of conventional gas production (Vandeweijer et al., 2011). The EGR process began by injecting produced CO_2 into the formation of this depleted gas reservoir, improving the gas recovery along with CO_2 sequestration. A Canadian depleted gas reservoir was also used for an EGR/CO_2 sequestration trial in 2002 but the operation was terminated after three years due to the early CO_2 breakthrough into the producing wells (Pooladi-Darvish et al., 2008). Both of these two EGR field trials were implemented in sandstone formations, and carbonate reservoirs have not yet been considered for any EGR projects, largely due to their inherent heterogeneity and fluid flow and transport complexity.

Whilst an accurate simulation lattice or model defining the field heterogeneity at the macro-scale is critical for the actual deployment of any reservoir simulation, fundamental system parameters are needed to describe the mixing process between injected CO_2 and natural gas. It has been shown that the physical description of transport at small scales can be important for field-scale behaviour, and therefore such descriptions have been used as fundamental inputs into large-scale simulations, including Multiple Rate Mass Transfer (MRMT) models (e.g. Haggerty et al., 2000)) and Continuous Time Random Walk (CTRW) based models (e.g. Rhodes et al., 2008)). While the early breakthrough of the solute at the field scale is caused by high permeability flow channels dominating at large length scale, diffusive retardation of solute plume at the pore scale may result in long residence times and is seen as prolonged tailing of the breakthrough curves (Gouze et al., 2008; Witthüser et al., 2003). One of the main contributions of our study is to demonstrate how complex carbonate pore structures with a significant portion of pore space at the sub-micron scale can have a different impact on the transport behaviour. This helps us better understand the nature of the influence that complex pore structures can have on the longer residence times observed in large-scale natural systems.

We recently presented the measured dispersion coefficients (K_L) of CO_2 and CH_4 for two sandstone cores (Berea and Donnybrook) over a range of pressure, temperature and interstitial velocities (Honari et al., 2013). Those highly reproducible data were used to obtain the characteristic mixing length for the sandstone samples and a generalized correlation was developed for reservoir simulators; however the data and hence the resulting correlation were

limited to the sandstone cores only. Extending that work to help address the lack of experimental studies of CO_2-CH_4 dispersion in carbonates was the primary motivation of the work presented here. The high accuracy achievable with this measurement approach also allowed recent theoretical developments for well-characterised carbonates and sandstones to be tested experimentally.

First, two carbonate rock samples (Ketton and Estaillades) were used to systematically measure pulse breakthrough curves for a range of pressures, temperatures and flow velocities. An analysis of the experimental results was then performed (using a multi-phase mass transfer model in one case) to extract the dispersion coefficients characteristic of the asymptotic regime. The results were interpreted in terms of the known pore-scale heterogeneity for each core, which has been measured using three independent techniques: mercury injection, NMR and X-ray CT. In addition, a new set of dispersion measurements was conducted for the Donnybrook sandstone core at very high interstitial velocities. These new sandstone data along with the carbonate results were used to examine the validity of the power law associated with dispersion in sandstones and carbonates reported by Bijeljic and Blunt (2006) and Bijeljic et al. (2011).

2. Literature Review

In this section, a summary of previous dispersion experiments for carbonate rocks is presented first. In particular, the long-tailed and early breakthrough curves reported for carbonates in the literature are reviewed and the proposed causes of these elongated breakthrough profiles are discussed to establish the most appropriate means of analysing the pulse breakthrough data for the Ketton carbonate presented here (e.g. Figure 1). Subsequently, the effect of heterogeneity on fluid flow behaviour within porous media including bead packs, sandstones and carbonates is reviewed in the context of establishing (a) the time scale required for the transition from non-Fickian (pre-asymptotic) to Fickian (or asymptotic) flow regimes and (b) the dependence of dispersion coefficient on velocity in the limit of high Péclet number.

2.1. Dispersion measurement in Carbonate rocks

Fluid transport through carbonate rocks has been studied for decades, with early breakthrough and long-tailed curves at later times having been found to be characteristics of these rock types. Brigham (1974) conducted step-input dispersion experiments for a carbonate core and reported long-tailed breakthrough curves. These were attributed to the

presence of existent dead end pores in the carbonate for which mass transfer rates were limited. Baker (1977) investigated the dispersion of benzene and meta-xylene by conducting step-change miscible displacement experiments through a vugular heterogeneous limestone (carbonate) core. The resultant effluent profiles indicated early breakthrough followed by long tailing, again presumably caused by stagnant regions. This type of breakthrough profile was also reported by Spence Jr. and Watkins (1980) who used xylene to miscibly displace iso-octane through San Andres carbonate cores from West Texas. Gist et al. (1990) measured dispersion coefficients by injecting a pulse of concentrated $NaCl_{(aq)}$ through consolidated rocks. Long tail breakthrough profiles appeared in two of the five carbonates tested. The macroscopic heterogeneity in permeability associated with the variability between those carbonate cores (i.e. heterogeneities on the length scale of 10^{-2} to 10^{-1} m) was considered to be the source of this anomalous behaviour rather than the width of the pore size distributions (which would be the basis of microscopic or intrinsic heterogeneity at the core scale).

Orr and co-workers systematically conducted miscible core flood experiments through four carbonates (Bretz and Orr Jr., 1987; Bretz et al., 1988; Orr Jr. and Taber, 1984). The cores were saturated with brine and step input or pulse experiments were conducted using a solution of the same brine containing 0.4% sucrose as the tracer. Even though the three carbonates produced early breakthrough curves with long tails, one of the cores showed more symmetric breakthrough profiles, similar to those observed for sandstone cores. The dispersion coefficients calculated for the carbonate rocks were also significantly greater than the ones obtained for the sandstones. They argued that the early breakthroughs for the three carbonates were caused not only by the widths of the measured pore size distribution but also by pore connectivity providing preferential flow paths.

The X-ray CT scanning approach has been also utilized to measure *in-situ* tracer concentration curves through several brine-saturated carbonate rock cores (Fourar and Radilla, 2009; Hidajat et al., 2004; Olivier et al., 2005). The early and long-tailed effluent breakthrough was the common signature for all resultant breakthrough profiles. This behavior was attributed to the heterogeneous characteristic of the carbonate rocks. For instance, Fourar and Radilla (2009) conducted tracer experiments at ambient conditions by saturating carbonate cores with a known NaCl brine and subsequently displacing it with a tracer consisting of a different NaCl concentration. The tracer concentrations as a function of time were measured both *in-situ* using X-ray CT and at the outlet of the core holder using a conductometer. The X-ray CT scanning provided the concentration profiles at several

locations along the cores, and showed the evolution of early and long tailed breakthrough profiles. These profiles were also consistent with the effluent long tailed breakthrough curves measured at the cores outlet using the conductometer.

Even though the flow of incompressible fluids through carbonate rocks has been broadly investigated, very few dispersion measurements have been conducted on gas-gas systems in carbonates (Batycky et al., 1982; Legatski and Katz, 1967; Mamora and Seo, 2002; Seo, 2004). Legatski and Katz (1967) initiated the gas-gas dispersion measurements in carbonate cores by conducting pulse dispersion experiments at ambient conditions and various interstitial velocities. Nitrogen pulses were injected into the argon-saturated cores and the dispersion coefficients were extracted. The dispersion was larger for the carbonates than the ones measured for sandstone samples; however the obtained dispersion values contained uncertainties of about 30%, based on the error bars shown explicitly in the reported figures.

Batycky et al. (1982) performed supercritical N_2-CH_4 displacement experiments on five carbonate cores at a pressure of 6.9 MPa and temperature of 23°C. Similar to other investigators, long tailed and early breakthrough profiles were detected during the course of their work, and were hypothesized to be the effect of stagnant pores. The resultant dispersion coefficients of carbonate samples were larger than the ones measured for Berea sandstone. Their experiments were only conducted for a maximum of three different flow velocities, which is insufficient for the development of a general correlation relating dispersion coefficient and velocity.

Seo and Mamora (Mamora and Seo, 2002; Seo, 2004; Seo and Mamora, 2005) measured breakthrough profiles for CH_4 displacement by CO_2 through a carbonate core at temperatures between 20 and 80°C and pressures between 3.5 and 20.5 MPa. The repeatability of the measured breakthrough profiles was limited due to the manual back pressure regulator used to control the core pressure (Seo, 2004). Several long-tailed breakthrough curves were observed during the course of their work and their attempts to appropriately regress these long-tailed profiles to the 1D-AD equation failed (Mamora and Seo, 2002; Seo, 2004).

2.2. Asymptotic and preasymptotic regimes in porous media

The one dimensional advective-dispersion (1D-AD) equation has been used widely to model solute transport through porous media:

$$\frac{\partial C}{\partial t} = K_{\mathrm{L}} \frac{\partial^2 C}{\partial x^2} - u \frac{\partial C}{\partial x}, \qquad (1)$$

Here C is the concentration of the dispersing species, K_{L} is the longitudinal dispersion coefficient and u is the mean interstitial velocity in the direction of bulk flow, x. This equation is a valid description of transport where the solute molecules quickly sweep over the whole potential velocity field within a chosen representative volume, as it occurs in Fickian processes. A narrow Gaussian spread of flow velocities is a signature of a Fickian process and is classically formed in homogeneous, unconsolidated bead packs (Blunt et al., 2013; Scheven et al., 2005). Thus, it is important to know whether the well-known asymptotic (Fickian) regime has been fully developed in various porous media prior to applying the 1D-AD equation. Prior to reaching this stage, the flow is considered to be pre-asymptotic (Bijeljic et al., 2004) and the time taken before this pre-asymptotic (or anomalous) behavior disappears is a function of the spatial heterogeneity of the porous media. In general, carbonate rocks are characterized as a more heterogeneous media than sandstone rocks and therefore require a longer time to reach the asymptotic regime. Recently, there have been extensive studies on pre-asymptotic dispersion in various porous media (Bijeljic et al., 2011, 2013a; Bijeljic et al., 2013b; Blunt et al., 2013; Mitchell et al., 2008; Scheven et al., 2007; Scheven et al., 2005). Most of these focused on velocities in the transition region or above (where the medium Péclet number, $Pe_{\mathrm{m}} = \frac{ud}{D}, > 1$ with D being the diffusion coefficient and d a characteristic length scale for mixing) to examine role of the porous media heterogeneity on the development of the pre-asymptotic and asymptotic flow regimes. For flow rates within the range of the diffusion-dominated region ($Pe_{\mathrm{m}} < 1$), this distribution of fluid displacement is Fickian-like and predominately dictated by restricted diffusion (Bijeljic et al., 2004; Gist et al., 1990; Levy and Berkowitz, 2003; Sahimi, 1995).

It was experimentally shown using NMR displacement propagator measurements that asymptotic flow in a column packed with 100 μm beads was achieved (at velocities of about 1 mm/s) when the solute travelled for a distance equivalent to only a few pores (Scheven et al., 2005). However, the pre-asymptotic regime for naturally consolidated sandstone and carbonate rocks was more persistent. Scheven et al. (2005) indicated that both types of rock cores consisted of large numbers of stagnant zones occupied by solute which did not completely diffuse out during the observation time of the NMR experiments conducted (Mitchell et al., 2008; Scheven et al., 2005). It was also shown that the stagnant regions in the

carbonate rock were larger and more persistent than those of the sandstones confirming that greater heterogeneity existed in the flow field within the carbonate rock (Mitchell et al., 2008; Scheven et al., 2005).

Pore network models have been initially developed to investigate fluid (water) flow through porous media at the pore scale (Bijeljic and Blunt, 2006; Bijeljic et al., 2004; Bruderer and Bernabe, 2001; Rhodes et al., 2009; Saffman, 1960; Sahimi et al., 1986), where the advective solute motion in the flow field is combined with random movements to account for molecular diffusion. The asymptotic dispersion predictions were in good agreement with experimental values for bead packs, sand packs and sandstones (Bijeljic et al., 2004; Rhodes et al., 2009). It was noted that, unlike bead packs, the solute molecules in sandstone network lattices at high Pe numbers (Pe>100) were required to travel through hundreds to thousands of pores before reaching the asymptotic regime. More recently, transport simulations directly on the voxels of 3D X-ray tomography images of various porous media have been presented (Bijeljic et al., 2011, 2013a; Bijeljic et al., 2013b; Blunt et al., 2013). The fluid flow and transport was modelled through a bead pack, Bentheimer sandstone and Portland carbonate rock cores similar to the ones used in NMR studies by Scheven et al. (2005) and Mitchell et al. (2008). The model's results were in excellent agreement with the NMR measurements for probability density functions of displacement (Bijeljic et al., 2011; Bijeljic et al., 2013b; Blunt et al., 2013). The investigation was expanded to cover a range of carbonate rocks (Bijeljic et al., 2013a), where the results demonstrated that the rocks with poor connectivity and a consequential wider range of velocities had more persistent preasymptotic behavior than those with better pore connectivity and narrower velocity distributions. This persistence of the non-Fickian transport behavior was attributed to the existence of correlated heterogeneity within those carbonates, which caused the fluid molecules to have to diffuse through many pores in which no flow was present so as to reach the high-flow channels.

The ratio of the dispersion coefficient to the diffusion coefficient, K_L/D, is commonly shown as a function of Pe_m; Equation (2) has been frequently used to describe this relationship:

$$\frac{K_L}{D} = \frac{1}{\tau} + Pe_m^n, \qquad (2)$$

Here τ is system tortuosity and n is an exponent. Different values of n have been reported in the literature such as $n = 1$ (Perkins and Johnston, 1963) and $1 < n < 1.4$ (Bijeljic et al. (2004)). It was found that the heterogeneity of the porous media causes the velocity

variations in the advection-dominated transport regime and controls the value of n, which is ~1.2 for sandpacks and sandstones ($10 < Pe_m < 600$) and ~1.4 for carbonates ($5 < Pe_m < 100$) (Bijeljic and Blunt, 2006; Bijeljic et al., 2011).

3. Methodology

3.1. Materials and Experimental method

Methane, carbon dioxide and nitrogen were supplied by BOC Scientific at purities higher than 0.999 mole fraction. Estaillades and Ketton carbonate rock cores, each 1.5 inch diameter and with lengths of 100-105 mm were used – the 2D cross sections of 3D micro-CT images of these carbonate rocks have been provided elsewhere (Bijeljic et al., 2013a; Tanino and Blunt, 2012). Berea and Donnybrook sandstone cores were also considered for reference purposes. The cores characterisations (dimensions, porosities, Φ, and permeabilities, k, at various confining pressures) are summarised in Table 1.

The core flood apparatus, shown in Figure 2, was designed to allow pulse injection experiments to be conducted through vertically-oriented cores at reservoir conditions as detailed by Hughes et al. (2012) and Honari et al. (2013). After being placed in the core holder, the core was initially saturated with CH_4 and pressurized to the test pressure using the injection syringe pump. A pre-mixed pulse of 50 mol% CH_4 and 50 mol% CO_2 was pressurized up to the experimental pressure, injected upstream of the core, and was carried through the core by CH_4 at the interstitial velocity specified. The composition of the core effluent was subsequently measured using a FT-IR spectrometer. The CH_4 injection was stopped when the complete breakthrough profile had been recorded and no trace of CO_2 was detected. These pulse experiments were conducted at pressures and temperatures of 8 to 14 MPa and 40 to 60 °C, respectively, and interstitial velocities ranging from 0.0036 to 3.56 mm s^{-1}. Since the critical pressures and temperatures of CO_2 and CH_4 are (31 °C, 7.38 MPa) and (-82.6 °C, 4.6 MPa) respectively (REFPROP, 2012), all tests were hence performed at supercritical conditions.

3.2. Data analysis

Levenspiel (1999) proposed the following solution to Equation (1) for pulse experiments with the following initial and boundary conditions:

$C(x > 0, t = 0) = 0$, $C(x = \infty, t) = 0$, $C(x = 0, 0 < t < T) = C_0$ and $C(x = 0, t > T) = 0$.

$$C = \frac{u}{\sqrt{4\pi K_{\mathrm{L}} t}} \exp\left(-\frac{\left(L - ut\right)^2}{4K_{\mathrm{L}} t} \right). \qquad (3)$$

Here T is the pulse duration and L is the experimental length scale (core length). The breakthrough profiles obtained for the Estaillades carbonate core were regressed to Equation (3) and the resultant fit quality was comparable to those obtained for sandstone cores during our previous studies (Honari et al., 2013).

However, Equation (3) alone was not adequate for description of the effluent tracer concentration curves produced from the Ketton carbonate, as shown in Figure 1, because of the non-Fickian/preasymptotic transport behavior associated with its heterogeneity in pore sizes. To describe this non-Fickian flow regime and its corresponding early and long-tailed breakthrough curves, several alternative models have been developed including the mobile-immobile model (MIM), diffusion models, MRMT models (Haggerty and Gorelick, 1995) and CTRW models (Berkowitz et al., 2006). In this case, it was found that the non-Fickian behavior of Ketton carbonate could be adequately modeled utilizing the MIM approach, which assumes the existence of two distinct regions in the rock, mobile and stagnant/immobile, and which describes the diffusional transport of species between these two zones using a first order mass transfer expression. This model was initially proposed by Deans (1963), who added two new parameters to Equation (1), namely the mass transfer coefficient and immobile volume fraction, but did not include the longitudinal dispersion coefficient. Coats and Smith (1964) modified Deans' version of Equation (1) by adding this dispersion coefficient to produce (Coats and Smith, 1964; Van Genuchten and Wierenga, 1976):

$$\theta_{\mathrm{m}} \frac{\partial C_{\mathrm{m}}}{\partial t} + \theta_{\mathrm{im}} \frac{\partial C_{\mathrm{im}}}{\partial t} = \theta_{\mathrm{m}} K_{\mathrm{L}} \frac{\partial^2 C_{\mathrm{m}}}{\partial x^2} - u_{\mathrm{m}} \theta_{\mathrm{m}} \frac{\partial C_{\mathrm{m}}}{\partial x}, \qquad (4)$$

$$\theta_{\mathrm{im}} \frac{\partial C_{\mathrm{im}}}{\partial t} = \beta\left(C_{\mathrm{m}} - C_{\mathrm{im}}\right) \qquad (5)$$

where C_{m} and C_{im} are the concentrations of the dispersing solute species in the mobile and immobile regions, respectively; θ_{m} and θ_{im} are the mobile and stagnant fractions of the fluid in the porous media; β is a mass transfer coefficient; and u_{m} is the mean interstitial velocity in the mobile zone. This model has been used for several dispersion studies on carbonate rocks (Baker, 1977; Batycky et al., 1982; Bretz and Orr Jr., 1987; Bretz et al., 1988; Brigham, 1974; Spence Jr. and Watkins, 1980). Equation (4) and (5) may be analytically solved for a

pulse input where semi-infinite initial-boundary conditions were assumed (Goltz and Roberts, 1986; van Swaaij, 1967; Villermaux and Van Swaaij, 1969):

$$\left(-K_{\mathrm{L}}\frac{\partial C_{\mathrm{m}}}{\partial x}+u_{\mathrm{m}}C_{\mathrm{m}}\right)_{x=0}=0,$$

$$\left(\frac{\partial C_{\mathrm{m}}}{\partial x}\right)_{x\to\infty}=0,$$

$$C_{\mathrm{m}}\left(x,0\right)=\frac{M}{\theta_{\mathrm{m}}}\delta\left(x\right),$$

$$C_{\mathrm{im}}\left(x,0\right)=0.$$

$$C_{\mathrm{m}}\left(x,t\right)=\exp\left(-\frac{\beta t}{\theta_{\mathrm{m}}}\right)G\left(x,t\right)+\frac{\beta}{\theta_{\mathrm{m}}}\int_0^t H\left(t,\tau\right)G\left(x,\tau\right)d\tau, \tag{6}$$

where

$$G\left(x,t\right)=\frac{M}{\theta_{\mathrm{m}}\sqrt{\pi K_{\mathrm{L}}t}}\exp\left(-\frac{\left(x-u_{\mathrm{m}}t\right)^2}{4K_{\mathrm{L}}t}\right)-\frac{u_{\mathrm{m}}M}{2\theta_{\mathrm{m}}K_{\mathrm{L}}}\exp\left(\frac{u_{\mathrm{m}}x}{K_{\mathrm{L}}}\right)erfc\left(\frac{x+u_{\mathrm{m}}t}{2\sqrt{K_{\mathrm{L}}t}}\right) \tag{7}$$

$$H\left(t,\tau\right)=\left(\frac{\theta_{\mathrm{m}}}{\theta_{\mathrm{im}}\left(t-\tau\right)\tau}\right)^{\frac{1}{2}}\times\exp\left(\frac{-\beta\left(t-\tau\right)}{\theta_{\mathrm{im}}}-\frac{\beta\tau}{\theta_{\mathrm{m}}}\right)\times\tau I_1\left[\frac{2\beta}{\theta_{\mathrm{im}}}\left(\frac{\theta_{\mathrm{im}}\left(t-\tau\right)\tau}{\theta_{\mathrm{m}}}\right)^{\frac{1}{2}}\right] \tag{8}$$

Here M is the injected pulse mass, δ(x) is Dirac delta function, τ is the integration variable and I_1 is a modified Bessel function of the first kind. To apply this solution to the measured effluent pulse profiles obtained for the Ketton core, the dispersion coefficient (K_{L}), the mobile fluid fraction (θ_{m}) and the mass transfer coefficient (β) were treated as the fitting parameters and the measured pulse breakthrough profiles were regressed to Equation (6).

As discussed above, the MIM was developed based on the existence of mobile and immobile regions, indicating the mixing process occurred at two different time scales (Haggerty and Gorelick, 1995).

Within the range of experimental flow velocities (0.011-2.32 mm·s^{-1}), the transit time for the injected pulse through the 105 mm long Ketton carbonate rock core is (45-9545) s. Given that the diffusion coefficient of CO_2 in CH_4 was in the range (8.1-16.4)×10^{-8} m^2.s^{-1}, this would correspond to a minimum root mean squared displacement due to diffusion over this time frame of 4.67 mm (according to the Stokes-Einstein equation). With reference to Figure 3, this significantly exceeds any length-scale evident in this X-ray CT image of the Ketton

rock core. Thus, it is hypothesized that the resultant dispersion coefficients (K_L) determined using the MIM for the Ketton carbonate in this study represent the asymptotic values.

Finally, the tubing upstream and downstream of the cores and the inhomogeneous velocity profiles at the core entrance and exit contribute additional mixing and erroneously increase the apparent dispersion. The correction for the erroneous contribution of these effects to dispersion associated with our experimental apparatus (as measured previously (Hughes et al. (2012) and Honari et al. (2013)) was applied to our new results. The concentration profiles were measured at the same conditions of *T*, *p* and flow rate for short and long Berea rock cores. Then, the breakthrough profiles of the short core were used as the initial inlet boundary condition for a hypothetical core extension equal to the length difference between long and short cores. A central finite difference method, implemented in Matlab (2008) (Version 7.7.0 R2008b), was used to numerically solve Equation (1) for this hypothetical core and regressed to the corresponding experimental long core data. Consequently, the systematic error, between the calculated long core dispersion (K_{long}) using Equation (3) and the resultant dispersion applying the above numerical method, was quantified. An average correction of 23% was found to be required and all data presented herein are the corrected longitudinal dispersion values (K_{corr}).

4. Results and Discussion

4.1. Repeatability and uncertainty in the experimental measurements

The reproducibility of the pulse breakthrough profiles through the carbonate rock cores were examined by replicating the flow experiments at various conditions. The relative standard deviations of calculated dispersion coefficients were consistently less than 9%. Figure 4(a) illustrates the two breakthrough curves from the Estaillades carbonate at 60 °C, 10 MPa and 0.14 $mm \cdot s^{-1}$ with their 1D-AD fit. Figure 4(b) shows two breakthrough profiles from the Ketton carbonate at 60 °C, 10 MPa and 0.28 $mm \cdot s^{-1}$ together with the results of both the 1D-AD and MIM fits. It is evident from Figure 4(b) that the 1D-AD fit failed to capture tail of the Ketton breakthrough curves whereas the MIM model was able to describe those experimental data adequately. The dispersion coefficients (K_{corr}) obtained for the repeat Estaillades pulse profiles were 1.46×10^{-7} $m^2 \cdot s^{-1}$ and 1.43×10^{-7} $m^2 \cdot s^{-1}$, with a root mean squared error (RMSE) in CO_2 mole fraction of 0.0005 between the measured data and the fitted breakthrough pulse; this RMSE is comparable to the instrumental noise floor of the experimental composition measurements. For the Ketton carbonate, the apparent dispersion values obtained from the 1D-AD fits were 5.92×10^{-7} $m^2 \cdot s^{-1}$ and 5.83×10^{-7} $m^2 \cdot s^{-1}$ with an

RMSE of about 0.001 mole fraction whereas the MIM fit resulted in dispersion coefficients of 4.03×10^{-7} $m^2\cdot s^{-1}$ and 3.91×10^{-7} $m^2\cdot s^{-1}$ with an RMSE of 0.0005. The statistical uncertainties of the K_L values obtained using Equation (3) for Estaillades and Equation (6) for Ketton were consistent with those obtained previously for sandstone cores (Honari et al., 2013), as were standard deviations of multiple repeat measurements. The nominal dispersivity (K_{corr}/v) for the Estaillades based on this data was ~1 mm and that for the Ketton was ~2.11 mm for the MIM fit. We note that these are similar and discuss this point further below with respect to Figure 9.

4.2. NMR distributions of T_2 relaxation for sandstones and carbonates

Figure 5(a) summarises the NMR distributions of T_2 (which is related to pore size, detailed by Latour et al. (1993), Latour et al. (1994) and Hurlimann et al. (1994)) relaxation for the Berea and Donnybrook sandstones and the Estaillades and Ketton carbonates. The Berea sandstone was characterized by a unimodal distribution of T_2 relaxation whereas Donnybrook showed a broader multimodal distribution. In our previous work, large proportions of the pores in these sandstones were demonstrated to be over one micron (Honari et al., 2013) and the relatively small numbers of micro pores observed was attributed to the presence of clay-bound water (Jorand et al., 2011; Straley et al., 1997). The distributions of T_2 relaxation for the carbonate rocks consisted of two distinct peaks, which was consistent with the pore size distributions previously reported (Bijeljic et al., 2013a; Tanino and Blunt, 2012). Figure 5(b), which is adapted from the data presented by Bijeljic et al. (2013a), illustrates the pore throat size distributions for Ketton and Estaillades carbonate rocks using the Mercury Injection Capillary Injection (MICP) approach. It shows two distinct peaks for both Estaillades and Ketton that is attributed to intra-aggregate pores and intra-particle pores. A large portion of the pore throat size for these carbonates are less than one micron. Importantly both the NMR and MICP data indicate that while both cores have bi-modal pore size distributions, the lower mode of the Ketton core is about an order of magnitude smaller in length scale than the lower mode of the Estaillades core.

4.3. Difference in sandstone and carbonate pulse breakthrough curves

Figure 6 compares the pulse breakthrough profiles of Berea and Donnybrook sandstones with the ones measured for Ketton and Estaillades carbonates at similar flow, temperature and pressure conditions. Our previous results showed the 1D-AD equation was adequate for the description of dispersion of CO_2-CH_4 system through Berea and Donnybrook sandstone cores

(Honari et al., 2013). Larger dispersion coefficients at similar conditions for Donnybrook sandstone were reported, indicating a higher level of heterogeneity relative to the homogenous Berea sandstone. Since carbonate rocks are known as heterogeneous porous media, long tailing and early breakthrough profile of the CO_2 together with comparatively higher dispersion coefficients were expected. After comparing several measured dispersion coefficients of the sandstones and carbonates at similar conditions, the dispersion coefficients for both carbonate samples were found to be larger than for the homogeneous sandstone rock (Berea) whereas Estaillades showed similar dispersive behaviour to the more heterogeneous (Donnybrook) sandstone. Ketton exhibited the greatest dispersion among all the core samples used during this study. The pulse breakthrough profiles we observed for Ketton carbonate showed a more persistent long tail and an earlier breakthrough (Figure 6-*right*) than for Estaillades carbonate, which produced breakthrough curves similar to those observed for Donnybrook sandstone. We note that this is not entirely consistent with the modelling studies of pre-asymptotic transport on *mm*-scale micro-CT images of carbonates (Bijeljic et al., 2013a), for which Estaillades was predicted to have more anomalous transport behaviour than Ketton.

There are several reasons for the discrepancy between the modelled preasymptotic transport in these cores and that observed here using supercritical CO_2 in methane. First, the modelling studies were based on direct simulation of transport in which the achievable resolution of the X-ray tomography did not allow consideration of microporosity (<1 micron). The NMR and MICP measurements (Figure 5) both indicate that the sub-micron pore sizes in Ketton are smaller by an order of magnitude than those in Estaillades. This will cause the diffusive transit times of molecules in a supercritical phase to be longer in the Ketton carbonate, leading to increased dispersion.

The difference in the degree of anomalous transport can also be ascribed to the difference in the phase of the fluid being injected into the carbonate core compared with that considered in the simulations (supercritical fluid vs liquid). This means that the relevant diffusion coefficient was about 2 orders of magnitude larger in our supercritical fluid experiments (Takahashi and Iwasaki, 1970) than in the modelling study of liquid transport, which has a significant impact on the time required to reach the asymptotic regime. Physically, the time scale taken to reach the asymptotic regime is that required for a particle to sample the entire medium's heterogeneity by molecular diffusion (Blunt et al., 2013). Thus, Blunt et al. (2013) calculated that a bulk fluid with a velocity of 1 mm s^{-1} and a diffusion time of 1000 s

(calculated based on 2 mm domain) needs to travel for several meters before the asymptotic flow condition can be formed. In contrast, since the interstitial velocities used for Estaillades carbonate during this study were limited from 0.0036 to 1.65 mm s^{-1} and the diffusion coefficient was 2 orders of magnitude larger, the asymptotic regime should have been achieved in our experiments with the Estaillades rock in about two centimetres.

We hypothesize that for our core flooding experiments with CO_2, the microporosity together with inter-aggregate (macro) pores enhanced the pore connectivity within the Estaillades core, accelerating the transition from the preasymptotic to asymptotic regime. Consequently, fully developed asymptotic flows were established in the Estaillades core and so the measured pulse breakthrough profiles could be adequately described by the 1D-AD equation. In contrast, since Ketton had the most well-connected pores at larger length scales (as evident in the XMT images) and also the smallest micro-pores indicated by the MICP measurements of pore size distribution (Bijeljic et al., 2013a; Tanino and Blunt, 2012) and by the NMR measurements in Section 4.2. Thus, we hypothesize that while bulk fluid flowed preferentially through Ketton's larger inter particle pores (very high permeable region), an appreciable number of CO_2 molecules travelled through to and from the intra-grain stagnant pores via extremely tortuous paths to reach the fast flow regions. This delayed the diffusion of CO_2 out of these micro -pores and the time required to reach the core outlet, causing long tail breakthrough profiles. Consequently, it demonstrated persistent flow behaviour in the preasymptotic regime.

Finally, the carbonate micro-CT images used in the modelling studies were significantly smaller (<5 mm domain) than the samples used during this study. As the carbonates are considered heterogeneous porous media at multiple scales, large variations in their pore network structures are, therefore, expected from one sample to another and also when the upscaling process from a smaller sample to a core-size sample is performed. Thus, this could lead to different results in various samples from the same carbonate formation.

The MIM model was adequately fit to the Ketton pulse breakthrough profiles using K_L, the mobile fluid fraction (θ_m) and the mass transfer coefficient (β) as the adjustable parameters. The θ_m data were approximately constant with the mean value of about 0.76 over the range of interstitial velocities whereas β increased linearly with increasing the interstitial velocity (Figure 7a). This indicates that as the flow velocity increased an insignificant reduction occurred with respect to the immobile fluid fraction. In contrast the increased velocity in the

mobile fraction resulted in a significantly reduced diffusion film length for exchange between the mobile and immobile fractions manifesting in an increase in β. This is consistent with the results of Johns et al. (2000) in which detailed 3D Magnetic Resonance Imaging (MRI) velocity measurements were acquired for flow through unconsolidated porous media. Those results revealed that the stagnant portion of the fluid was relatively constant as flow rate was increased, whereas the velocity profile in the individual (mobile) pores increased and flattened, consistent with an increased value of β. Figure 7b indicates that the mass transfer coefficients obtained in this study were comparatively consistent with the ones described in literature (Baker, 1977; Batycky et al., 1982; Bretz and Orr Jr., 1987; Orr Jr. and Taber, 1984; Spence Jr. and Watkins, 1980). The resultant corrected dispersion coefficients (K_{corr}) and their corresponding experimental conditions (T, p and u_m) for the Estaillades and Ketton carbonates, as well as new high velocity data obtained for the Donnybrook sandstone, are listed in Table 2.

In our previous work (Honari et al., 2013), the dispersivity of consolidated rocks (α) was identified as the characteristic length scale (d) that should be used in the calculation of Pe_m. Thus, the dispersion values for the examined sandstones were plotted against interstitial velocities and the dispersivities were calculated using Equation (2) where the value of n was equal to 1 (see Figure 4 from Honari et al. (2013) for more detail). To determine the dispersivity of a porous medium by regression of Equation (2) to dispersion coefficients measured as a function of velocity, the value of n must be held constant because of the parameter correlation between it and α. The dispersivities for Berea and Donnybrook sandstones and Estaillades and Ketton carbonates were again determined using Equation (2) but in this work n was constrained to be either 1.2 or 1.4 for the sandstone and carbonate rocks, respectively. These exponents have been shown by simulations to better represent the different advective mixing behaviour exhibited by these types of rock in the limit of high Pe_m as a result of their different heterogeneities (Bijeljic and Blunt, 2006; Bijeljic et al., 2011). As discussed below, while the difference between exponent values at moderate Pe_m on the predicted dispersion is small, at high Pe_m numbers it is significant. Figure 8 illustrates the determination of the dispersivities using the larger exponents for sandstones and carbonates, while Table 3 lists the values of α determined from the dispersion coefficient data using the various power law exponents. The results show that: (a) the larger exponents for both types of rock result in reduced estimates of the characteristic mixing lengths, particularly for cores where dispersion was measured at high interstitial velocities, and (b) once the larger exponent

for the carbonates is accounted for, their characteristic mixing lengths are actually slightly smaller than that of Donnybrook sandstone. This result is broadly consistent with the NMR distributions shown in Figure 5(a).

The calculated dispersivities were then used to produce Figure 9(a) where the ratios of dispersion and diffusion coefficients, K_{corr}/D, were plotted against Pe_m. The data from this study and the ones obtained previously (Honari et al., 2013) were included in the plot together with two curves utilizing Equation (2) where n was 1 for $Pe_m<1$ and 1.2 and 1.4 (power-law scaling) for $Pe_m>1$. Figure 9(a) explicitly shows that the curves produced using Equation (2) with n = 1.2 for sandstones and n = 1.4 for carbonates are consistent with the new sets of Donnybrook and Ketton data obtained at $Pe_m>10$, which provides experimental support for the power law exponents derived from transport simulations (e.g. Bijeljic and Blunt (2006) and Bijeljic et al. (2011)).

To further examine the improvement obtained by the power law, the alternative dispersivity values calculated with the constraint n = 1 in Equation (2) were used to investigate the effect of this assumption at high Pe_m numbers. The right panel of Figure 9(b) shows the K_{corr}/D data measured for all cores at $Pe_m > 10$ plotted against values of Pe_m calculated using these alternative dispersivities (the first row of Table 3). It is apparent that for $Pe_m > 45$ a power law with n = 1 can no longer describe the data adequately. In contrast, the left panel of Figure 9(b) shows that the K_{corr}/D data for sandstone and carbonates are better represented over the entire range using power law exponents of n = 1.2 and 1.4, respectively, together with the corresponding mixing length scales shown in the second and third rows of Table 3.

Finally, we note that in the diffusion dominated regime ($Pe_m<1$) transport behaviour in Ketton carbonate was somewhat different to the other three rock cores, exhibiting higher dispersion coefficients with an inflection point apparent near Pe_m = 0.2. At these low values of Pe_m, the impact of the immobile fraction (~20 % - see Figure 7) on the measured dispersion is significantly smaller, as indicated by the reduced mass transfer coefficients. One possible explanation for the higher dispersion coefficients in the diffusion dominated regime is that the immobile fraction largely resides in the micropores of the Ketton carbonate, and that these are not well connected with flow paths through the core. Instead, we hypothesise that the mode of larger pores (> 10 μm) in the Ketton are well-connected and provide a less tortuous flow path that does not restrict the diffusive length scale probed during longer time periods to the same extent as occurs in the other cores.

5. Conclusions

The impact of rock heterogeneity on the dispersion of supercritical CO_2 in CH_4 has been extensively studied using well characterised carbonate and sandstone cores over a large range of Péclet numbers. Both carbonates had bimodal pore size distributions with one of the modes corresponding to appreciable micro-porosity. However, only the Ketton carbonate, which had the larger separation between the PSD modes and intra-grain micropores with pore throats below 0.1 μm, exhibited persistent preasymptotic transport behaviour with an early breakthrough and subsequent long-tailed profiles. This observation to some extent differed from the results of recent sophisticated transport simulations for these two carbonate cores because of the limited spatial resolution of the X-ray CT images used to develop the models. In addition, diffusion in supercritical CO_2 is more rapid than in liquid water, which causes the transport observed on the time scales of these experiments to be more sensitive to the rock's micro-porosity.

By using a mobile-immobile model to analyse the breakthrough profiles observed for the Ketton carbonate, asymptotic dispersion coefficients were obtained and compared with similar dispersion coefficients determined for the other cores using the 1D advective dispersion equation. Measurements at high Pe_m showed that, consistent with the results of transport simulations, power law exponents of $n = 1.2$ and $n = 1.4$ should be used to describe dispersion in sandstones and carbonates, respectively. With these exponents, the dispersivities (mixing length scales) of the carbonates (0.6 mm) were nearly twice as large as that of homogenous Berea sandstone (0.36 mm) but slightly smaller than that of Donnybrook sandstone (0.85 mm). This is broadly consistent with the widths of the pore size distributions for these four cores measured by NMR and MICP. In the diffusive regime ($Pe_m < 1$), the Ketton core exhibited greater dispersion than the other cores, suggesting its larger (inter-grain) pores were well connected and provided a flow path of relatively low tortuosity. This work demonstrates how the dispersion of CO_2 in complex carbonate cores can be assessed and correlated to account for the effects of pressure, temperature, composition, velocity, and rock heterogeneity to enable accurate simulations of Enhanced Gas Recovery.

6. Acknowledgment

This work was supported by the Western Australian Department of Environment Regulation through the Low Emissions Energy Development fund. EFM thanks the Departments of Chemical Engineering and Earth Sciences and Engineering at Imperial College for both a

stimulating sabbatical and helping to initiate this collaborative research effort. BB would like to thank the EPSRC (grant EP/L012251/1) for financial support.

7. References

Adepoju, O.O., Lake, L.W., Johns, R.T., 2013. Investigation of anisotropic mixing in miscible displacements. SPE Reservoir Evaluation & Engineering 16, 85-96.

Ahlbrandt, T.S., Charpentier, R.R., Klett, T.R., Schmoker, J.W., Schenk, C.J., Ulmishek, G.F., 2005. AAPG Memoir 86 - Global resource estimates from total petroleum systems. American Association of Petroleum Geologists, Tulsa, Oklahoma.

Akbar, M., Vissapragada, B., Alghamdi, A.H., Allen, D., Herron, M., Carnegie, A., Dutta, D., Olesen, J.-R., Chourasiya, R.D., Logan, D., Stief, D., Netherwood, R., Russell, S.D., Saxena, K., 2000. A snapshot of carbonate reservoir evaluation Oilfield Review 12, 20-41.

Alvarado, V., Manrique, E.J., 2010. Enhanced oil recovery: an update review. Energies 3, 1529-1575.

Arya, A., Hewett, T.A., Larson, R.G., Lake, L.W., 1988. Dispersion and reservoir heterogeneity SPE Reservoir Eng. 3, 139-148.

Baker, L.E., 1977. Effects of dispersion and dead-end pore volume in miscible flooding. SPE Journal 17, 219-227.

Batycky, J.P., Maini, B.B., Fisher, D.B., 1982. Simulation of miscible displacement in full-diameter carbonate cores. Society of Petroleum Engineers Journal 22, 647-657.

Berkowitz, B., Cortis, A., Dentz, M., Scher, H., 2006. Modeling non-fickian transport in geological formations as a continuous time random walk. Reviews of Geophysics 44, 1-49.

Bijeljic, B., Blunt, M.J., 2006. Pore-scale modeling and continuous time random walk analysis of dispersion in porous media. Water Resources Research 42, W01202.

Bijeljic, B., Mostaghimi, P., Blunt, M.J., 2011. Signature of non-Fickian solute transport in complex heterogeneous porous media. Physical Review Letters 107, 204502.

Bijeljic, B., Mostaghimi, P., Blunt, M.J., 2013a. Insights into non-Fickian solute transport in carbonates. Water Resources Research 49, 2714-2728.

Bijeljic, B., Muggeridge, A.H., Blunt, M.J., 2004. Pore-scale modeling of longitudinal dispersion. Water Resources Research 40, W11501.

Bijeljic, B., Raeini, A., Mostaghimi, P., Blunt, M.J., 2013b. Predictions of non-Fickian solute transport in different classes of porous media using direct simulation on pore-scale images. Physical Review E 87, 013011.

Blunt, M.J., Bijeljic, B., Dong, H., Gharbi, O., Iglauer, S., Mostaghimi, P., Paluszny, A., Pentland, C., 2013. Pore-scale imaging and modelling. Advances in Water Resources 51, 197-216.

Bretz, R.E., Orr Jr., F.M., 1987. Interpretation of miscible displacements in laboratory cores. SPE Reservoir Eng. 2, 492-500.

Bretz, R.E., Specter, R.M., Orr Jr., F.M., 1988. Effect of pore structure on miscible displacement in laboratory cores. SPE Reservoir Eng. 3, 857-866.

Brigham, W.E., 1974. Mixing Equations in Short Laboratory Cores. Society of Petroleum Engineers Journal 14, 91-99.

Bruderer, C., Bernabe, Y., 2001. Network modeling of dispersion:Transition from Taylor dispersion in homogeneous networks to mechanical dispersion in very heterogeneous ones. Water Resources Research 37, 897-908.

Coats, K.H., Smith, B.D., 1964. Dead-end pore volume and dispersion in porous media. SPE Journal 4, 73-84.

Coats, K.H., Whitson, C.H., Thomas, L.K., 2009. Modeling Conformance as Dispersion. SPE Reservoir Evaluation & Engineering 12, 33-47.

Deans, H.A., 1963. A mathematical model for dispersion in the direction of flow in porous media Society of Petroleum Engineers Journal 3, 49-52.

Fourar, M., Radilla, G., 2009. Non-Fickian description of tracer transport through heterogeneous porous media. Transport in Porous Media 80, 561-579.

Gist, G.A., Thompson, A.H., Katz, A.J., Higgins, R.L., 1990. Hydrodynamic dispersion and pore geometry in consolidated rock. Physics of Fluids A 2, 1533-1544.

Goltz, M.N., Roberts, P.V., 1986. Three-dimensional solutions for solute transport in an infinite medium with mobile and immobile zones. Water Resources Research 22, 1139-1148.

Gouze, P., Le Borgne, T., Leprovost, R., Lods, G., Poidras, T., Pezard, P., 2008. Non-Fickian dispersion in porous media: 1. Multiscale measurements using single-well injection withdrawal tests. Water Resources Research 44, W06426.

Haggerty, R., Gorelick, S.M., 1995. Multiple-rate mass transfer for modeling diffusion and surface reactions in media with pore-scale heterogeneity. Water Resources Research 31, 2383-2400.

Haggerty, R., McKenna, S.A., Meigs, L.C., 2000. On the late-time behavior of tracer test breakthrough curves. Water Resources Research 36, 3467-3479.

Hidajat, I., Mohanty, K.K., Flaum, M., Hirasaki, G., 2004. Study of vuggy carbonates using NMR and X-Ray CT scanning SPE Reservoir Evaluation & Engineering 7, 365-377.

Honari, A., Hughes, T.J., Fridjonsson, E.O., Johns, M.L., May, E.F., 2013. Dispersion of supercritical CO_2 and CH_4 in consolidated porous media for enhanced gas recovery simulations. International Journal of Greenhouse Gas Control 19, 234-242.

Hughes, T.J., Honari, A., Graham, B.F., Chauhan, A.S., Johns, M.L., May, E.F., 2012. CO_2 sequestration for enhanced gas recovery: new measurements of supercritical CO_2-CH_4 dispersion in porous media and a review of recent research. International Journal of Greenhouse Gas Control 9, 457-468.

Hurlimann, M.D., Helmer, K.G., Latour, L.L., Sotak, C.H., 1994. Restricted diffusion in sedimentary rocks. determination of surface-area-to-volume ratio and surface relaxivity. Journal of Magnetic Resounance, Series A 111, 169-178.

Johns, M.L., Sederman, A.J., Bramley, A.S., Gladden, L.F., Alexander, P., 2000. Local transitions in flow phenomena through packed beds identified by MRI. AIChE Journal 46, 2151-2161.

Jorand, R., Annick, F., Koch, A., Clauser, C., 2011. Study of the variation of thermal conductivity with water saturation using nuclear magnetic resonance. Journal of Geophysical Research 116, B08208.

Lake, L.W., 1989. Enhanced oil recovery. Prentice Hall, New Jersey, USA.

Latour, L.L., Mitra, P.P., Kleinberg, R.L., Sotak, C.H., 1993. Time-dependent diffusion coefficient of fluids in porous media as a probe of surface-to-volume ratio. Journal of Magnetic Resounance, Series A 101, 342-346.

Latour, L.L., Svoboda, K., Mitra, P.P., Sotak, C.H., 1994. Time-dependent diffusion of water in a biological model system. Proceedings of the National Academy of Sciences of the United States of America 91, 1229-1233.

Legatski, M.W., Katz, D.L., 1967. Dispersion coefficients for gases flowing in consolidated porous media. SPE Journal 7, 43-53.

Levenspiel, O., 1999. Chemical reaction engineering, 3rd ed. John Wiley & Sons.

Levy, M., Berkowitz, B., 2003. Measurement and analysis of non-Fickian dispersion in heterogeneous porous media. Journal of Contaminant Hydrology 64, 203-226.

Mamora, D.D., Seo, J.G., 2002. Enhanced Gas Recovery by Carbon Dioxide Sequestration in Depleted Gas Reservoirs, SPE Annual Technical Conference and Exhibition. Society of Petroleum Engineers, San Antonio, Tx, pp. 1-9.

Manrique, E.J., Muci, V.E., Gurfinkel, M.E., 2007. EOR field experiences in carbonate reservoirs in the United States. SPE Reservoir Evaluation & Engineering 10, 667-686.

Matlab, version 7.7.0, 2008. The MathWorks Inc., Natick, Massachusetts

Mitchell, J., Graf von der Schulenburg, D.A., Holland, D.J., Fordham, E.J., Johns, M.L., Gladden, L.F., 2008. Determining NMR flow propagator moments in porous rocks without the influence of relaxation. Journal of Magnetic Resonance 193, 218-225.

Olivier, P., Cantegral-Gassiot, L., Laveissiere, J., Guillonneau, N., 2005. Analysis of multiphase flow behavior in vugular carbonates using X-Ray CT scanning. Petrophysics 46, 424-433.

Orr Jr., F.M., Taber, J.J., 1984. Displacement of oil by carbon dioxide, U.S. DOE, p. 255.

Peaceman, D.W., 1977. Fundamentals of numerical reservoir simulation. Elsevier, Amsterdam, The Netherlands.

Perkins, T.K., Johnston, O.C., 1963. A Review of Diffusion and Dispersion in Porous Media. Society of Petroleum Engineers Journal 3, 70-84.

Pooladi-Darvish, M., Hong, H., Theys, S., Stocker, R., Bachu, S., Dashtgard, S., 2008. CO_2 injection for enhanced gas recovery and geological storage of CO_2 in the long Coulee Glauconite F pool, Alberta, in: SPE (Ed.), SPE Annual Technical Conference and Exhibition, Denver, Colorado.

REFPROP, Version 9.0, 2012. The National Institute of Standards and Technology (NIST), Boulder Colorado

Rhodes, M.E., Bijeljic, B., Blunt, M.J., 2008. Pore-to-field simulation of single-phase transport using continuous time random walks. Advances in Water Resources 31, 1527-1539.

Rhodes, M.E., Bijeljic, B., Blunt, M.J., 2009. A rigorous pore-to-field-scale simulation method for single-phase flow based on continuous-time random walks. SPE Journal 14, 88-94.

Roehl, P.O., Choquette, P.W., 1985. Carbonate petroleum reservoirs. Springer New York.

Saffman, P.G., 1960. Dispersion due to molecular diffusion and macroscopic mixing in flow through a network of capillaries. Journal of Fluid Mechanics 7, 194-208.

Sahimi, M., 1995. Flow and transport in porous media and fractured rock: from classical methods to modern approaches. John Wiley, Weinheim.

Sahimi, M., Hughes, B.D., Scriven, L.E., Davis, H.T., 1986. Dispersion in flow through porous media: 1. One-phase flow. Chemical Engineering Science 41, 2103-2122.

Scheven, U.M., Harris, R., Johns, M.L., 2007. Intrinsic Dispersivity of Randomly Packed Monodisperse Spheres. Physical Review Letters 99.

Scheven, U.M., Verganelakis, D., Harris, R., Johns, M.L., Gladden, L.F., 2005. Quantitative nuclear magnetic resonance measurements of preasymptotic dispersion in flow through porous media. Physics of Fluids 17, 117107.

Seo, J.G., 2004. Experimental and Simulation Studies of Sequestration of Supercritical Carbon Dioxide in Depleted Gas Reservoirs, Petroleum Engineering. Texas A&M University, College Station, Tx, p. 119.

Seo, J.G., Mamora, D.D., 2005. Experimental and Simulation Studies of Sequestration of Supercritical Carbon Dioxide in Depleted Gas Reservoirs. Journal of Energy Resources Technology 127, 1-6.

Spence Jr., A.P., Watkins, R.W., 1980. The effect of microscopic core heterogeneity on miscible flood residual oil saturation SPE Annual Technical Conference and Exhibition, Dallas, Texas.

Straley, C., Rossini, D., Vinegar, H., Tutunjian, P., Morris, C., 1997. Core analysis by low field NMR. The Log Analyst 38, 84-95.

Takahashi, S., Iwasaki, H., 1970. The Diffusion of Gases at High Pressures. III. The Diffusion of $^{14}CO_2$, in the $^{12}CO_2$-CH_4 System. Bulletin of the Chemical Research Institute of Non-aqueous Solutions, Tohoku University 20, 27-36.

Tanino, Y., Blunt, M.J., 2012. Capillary trapping in sandstones and carbonates: Dependence on pore structure. Water Resources Research 48, W08525.

Van Genuchten, M.T., Wierenga, P.J., 1976. Mass transfer studies in sorbing porous media I. analytical solutions. Soil Science Society of America Journal 40, 473-480.

van Swaaij, W.P.M., 1967. Residence time distributions in Raschig ring columns at trickle flow Department of Chemical Engineering. Technische Hogeschool Eindhoven Technische Hogeschool Eindhoven

Vandeweijer, V., van der Meer, L.G.H., Hofstee, C., Mulders, F., Graven, H., D'Hoore, D. Monitoring CO_2 Injection at K12-B http://www.co2geonet.com/UserFiles/file/Open%20Forum%202011/PDF-presentations/2-10_Vanderweijer.pdf. (accessed Aug 21, 2011).

Villermaux, J., Van Swaaij, W.P.M., 1969. Modèle représentatif de la distribution des temps de séjour dans un réacteur semi-infini à dispersion axiale avec zones stagnantes. Application à

l'écoulement ruisselant dans des colonnes d'anneaux Raschig. Chemical Engineering Science 24, 1097-1111.
Witthùser, K., Reichert, B., Hötzl, H., 2003. Contaminant transport in fractured chalk: Laboratory and field experiments. Ground Water 41, 806-815.

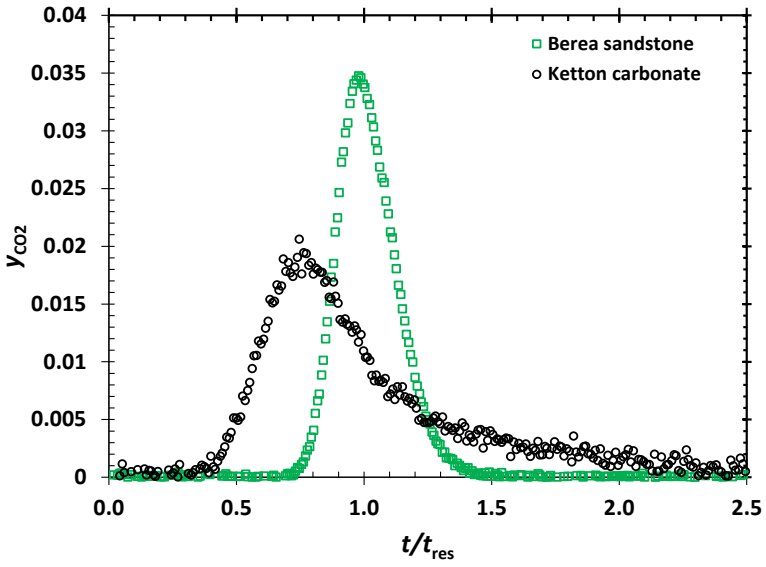

Figure 1. Pulse breakthrough curves measured for Berea sandstone and Ketton carbonate at 40 °C, 10 MPa with an interstitial velocity of 0.22 mm s^{-1}. The result for the carbonate core exhibits an early breakthrough followed by a long-tailed profile, characteristic of a mass transfer limitation between regions in the core where fluid was mobile and immobile.

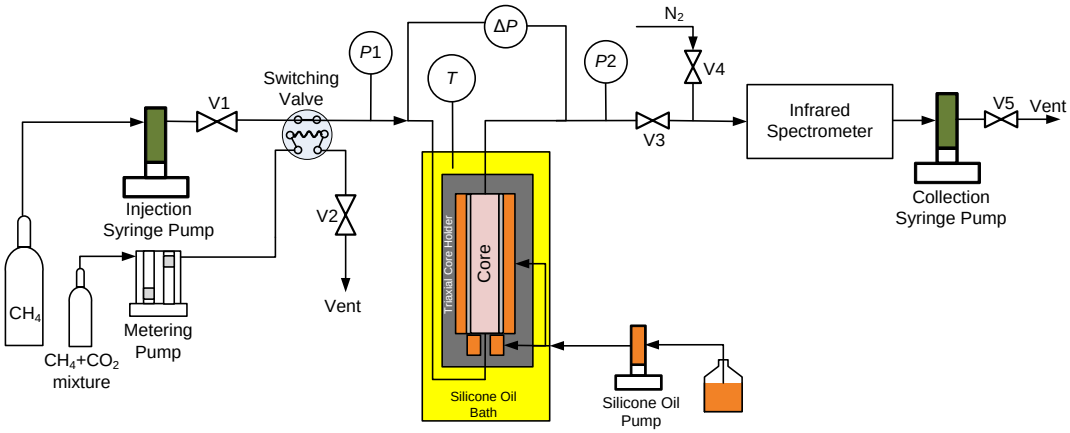

Figure 2. Schematic of the core flooding apparatus used to conduct the pulse-breakthrough measurements.

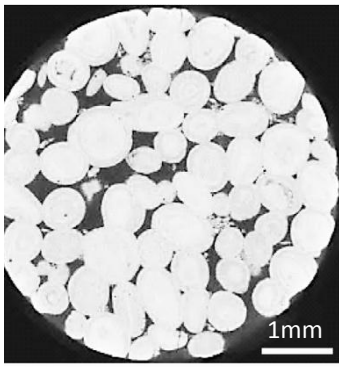

Figure 3. A two-dimensional cross section of three-dimensional X-ray scans of the Ketton carbonate with 5 mm diameter (adapted from Tanino and Blunt, 2012).

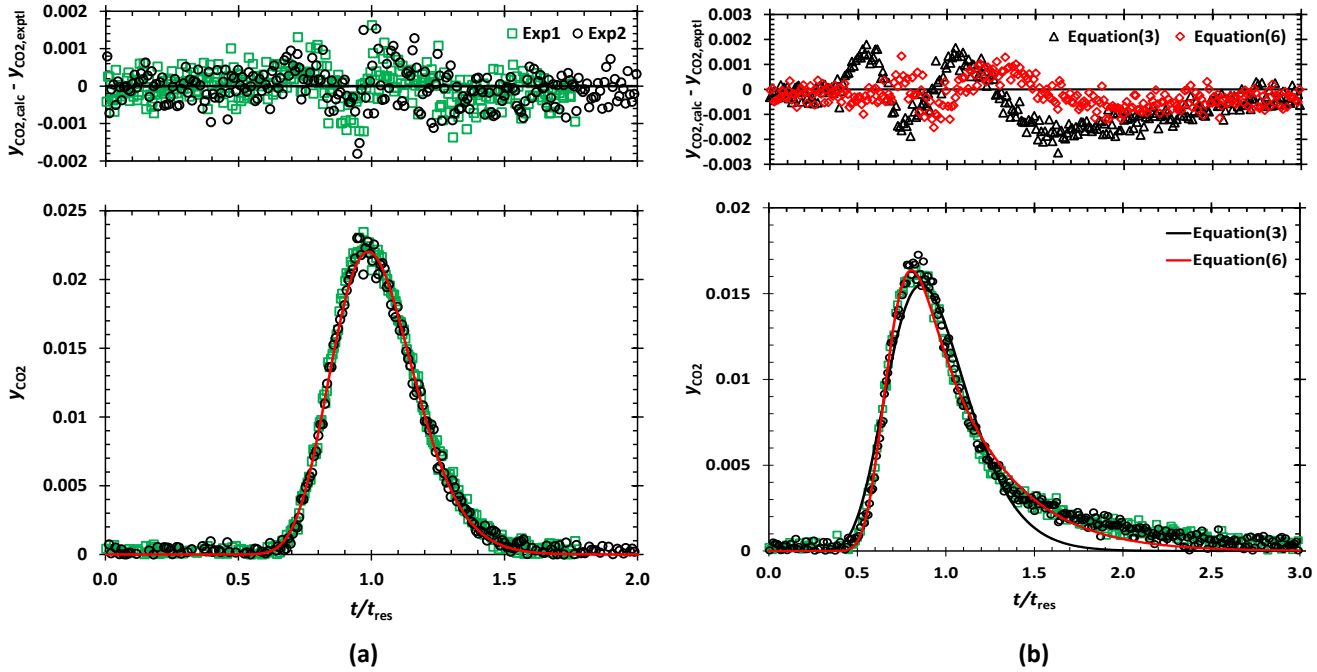

Figure 4. Repeatability of the pulse-breakthrough profiles for **(a)** Estaillades carbonate core at 60 °C, 10 MPa and 0.14 mm s^{-1} and **(b)** Ketton carbonate core at 60 °C, 10 MPa and 0.28 mm s^{-1}. The lower panel demonstrates the breakthrough profiles and the fits achieved using Equation (3) for Estaillades and both Equation (3) and (6) for Ketton. The upper panel shows the resulting residuals of the fits.

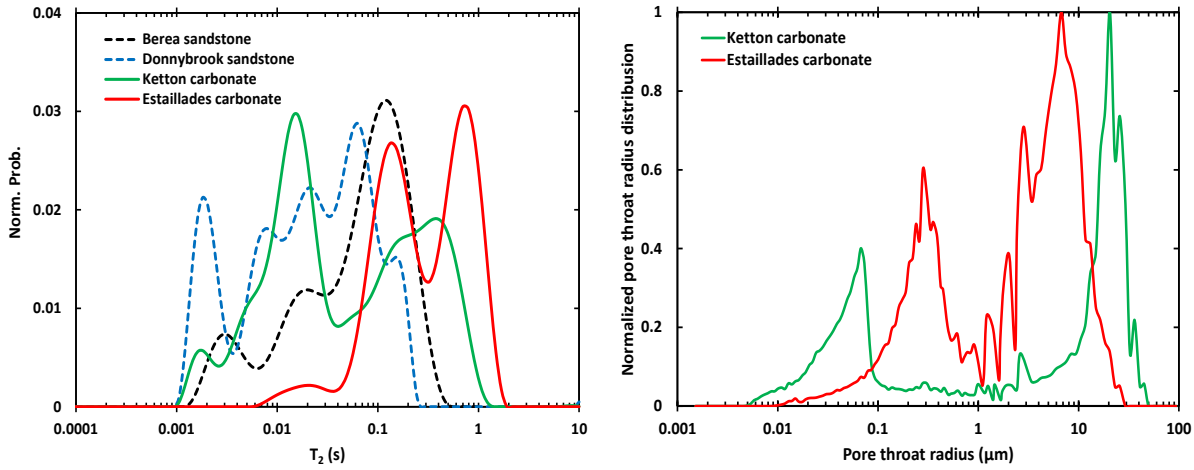

(a) **(b)**

Figure 5. (a) Distributions of T_2 relaxation for Berea and Donnybrook sandstone and Estaillades and Ketton carbonate rocks at fully saturated conditions. **(b)** Distributions of pore throat size obtained by MICP method for Estaillades and Ketton carbonates (adapted from Bijeljic et al., 2013a).

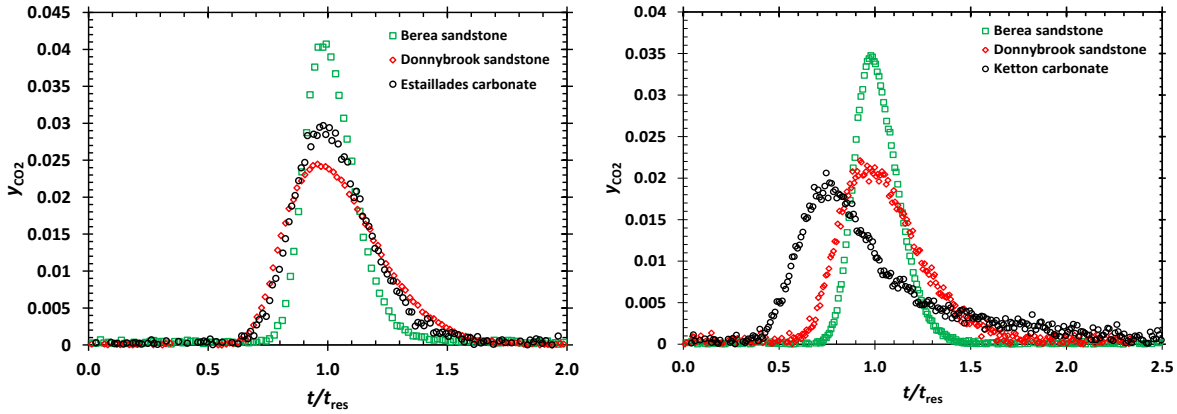

Figure 6. Comparison of the pulse breakthrough profiles obtained for Estaillades carbonate core (*left*) with those of Berea and Donnybrook sandstones at 60 °C, 10 MPa and mean interstitial velocity of 0.45 mm s^{-1}, and Ketton carbonate core (*right*) with those of Berea and Donnybrook sandstones at 40 °C, 10 MPa and mean interstitial velocity of 0.22 mm s^{-1}.

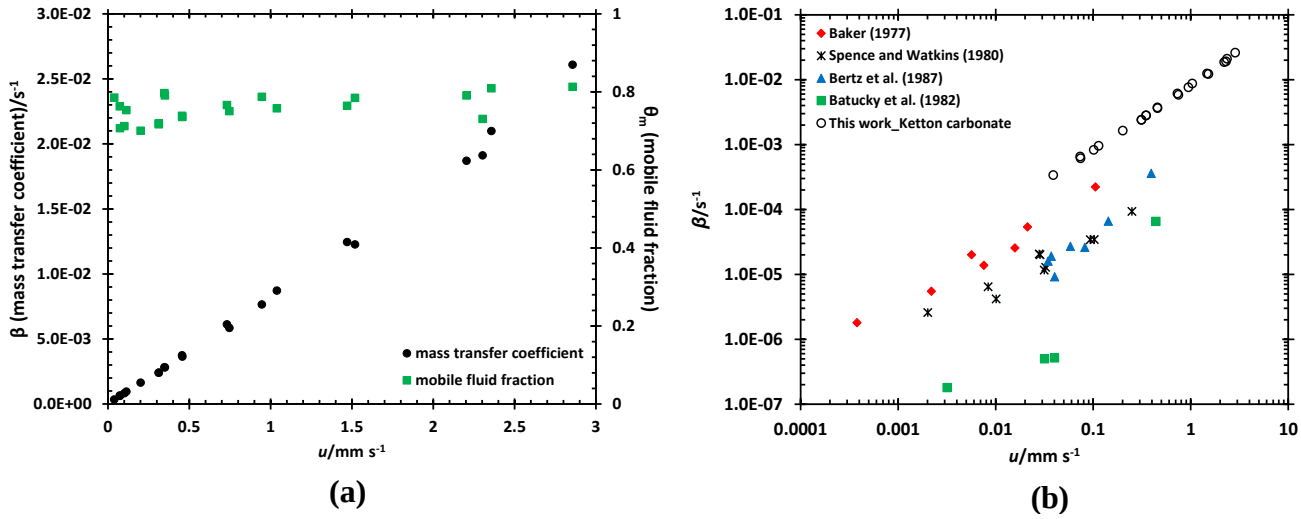

Figure 7. (a) Mass transfer coefficient and mobile fluid fraction as a function of interstitial velocity defined in Equation (6) for Ketton carbonate; **(b)** mass transfer coefficient obtained for Ketton carbonate along with the results reported for carbonate rocks in literature.

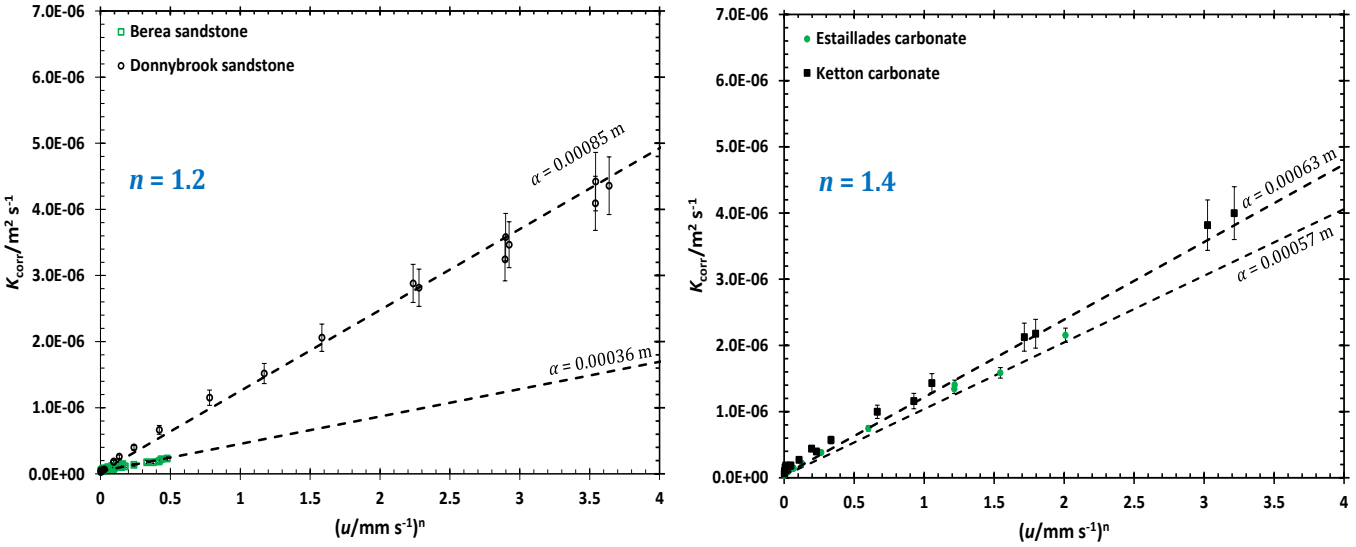

Figure 8. Variation of dispersion coefficients for Berea and Donnybrook sandstones (*left*) and Estaillades and Ketton carbonates (*right*) as a function of interstitial velocity.

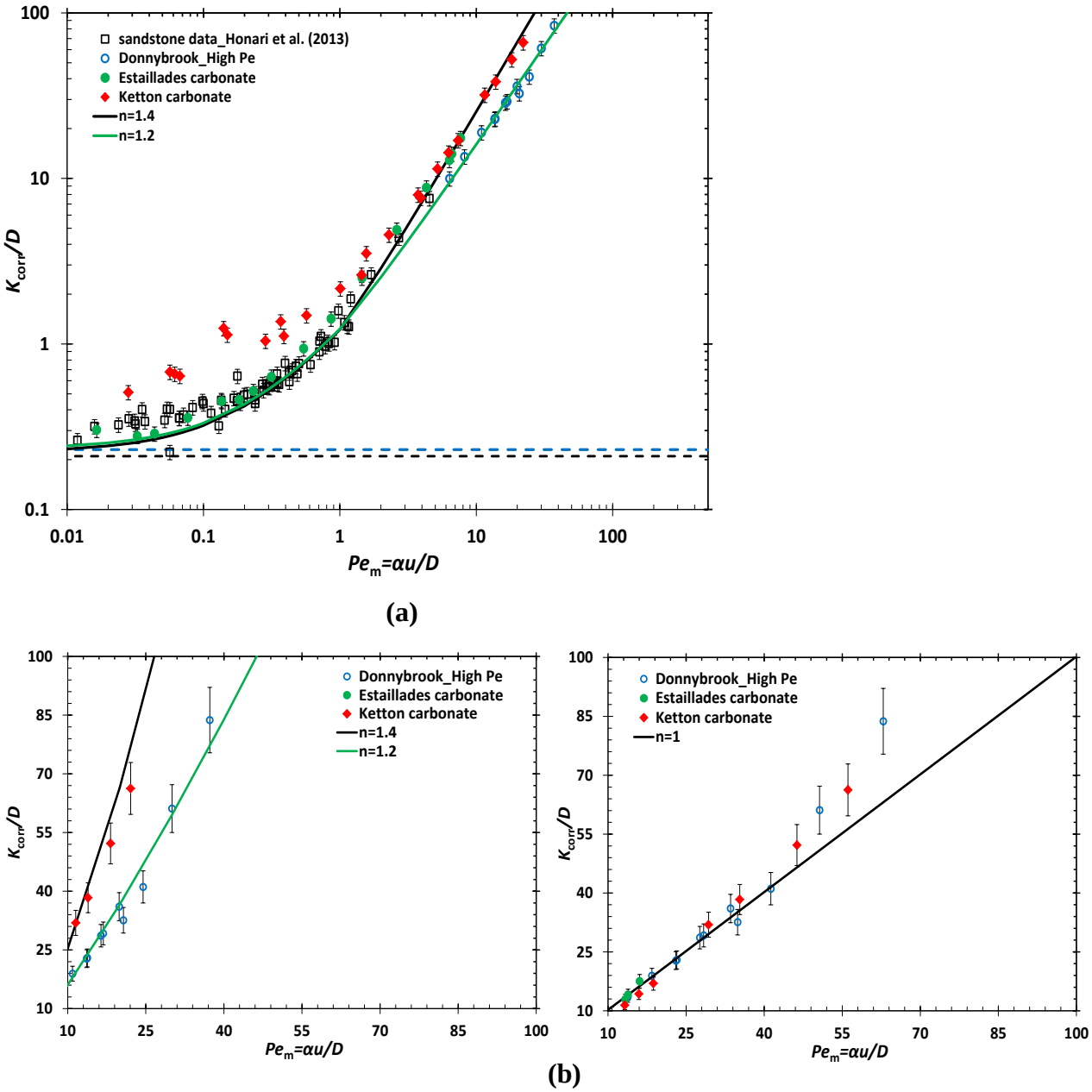

Figure 9. (a) Measured K_{corr}/D vs. Pe_m for Berea and Donnybrook sandstone and Ketton and Estaillades carbonate cores. The dashed lines indicate the independent NMR measurements of sandstone rocks tortuosity. The fitted curves are produced by Equation (2) for n equal to 1.2 and 1.4. **(b)** The data were analysed using Equation (2) (*left*) where n was equal to 1.2 (sandstones) and 1.4 (Carbonates) compared to (*right*) where n was 1.

Table 1. Rock core properties.

Core	Length (mm)	Diameter (mm)	$p_{confining}$ (MPa)	Φ	k (mD)
Berea sandstone	100.4	37.6	8	0.2043	463.3
			10	0.2039	460.7
			12	0.2036	458.2
Donnybrook sandstone	101.0	37.5	8	0.1576	12.07
			10	0.1573	12.01
			12	0.1572	11.95
Estaillades carbonate	105.6	37.9	8	0.2817	211.7
			10	0.2811	211.0
			12	0.2806	210.1
Ketton carbonate	104.7	38.0	8	0.2277	2922.4
			10	0.2274	2912.2
			12	0.2270	2902.7

Table 2. Dispersion coefficients of CO_2 - CH_4 for **(a)** Estaillades carbonate and Donnybrook sandstone and **(b)** Ketton carbonate.

(a)

Core	***T* (°C)**	***P* (MPa)**	***u* (mm s^{-1})**	***D* (10^{-8} m^2 s^{-1})**	***K*$_{corr}$ (10^{-8} m^2 s^{-1})**
Estaillades	40	8	0.066	16.4	8.50
	40	8	0.090	16.4	10.38
	40	10	0.004	12.5	3.79
	40	10	0.040	12.5	5.76
	40	12	0.024	10.0	4.49
	40	12	1.151	10.0	140.03
	60	10	0.009	15.2	4.22
	60	10	0.012	15.2	4.36
	60	10	0.144	15.2	14.39
	60	10	0.230	15.2	21.59
	60	10	0.387	15.2	38.18
	60	10	0.696	15.2	74.39
	60	10	1.149	15.2	133.65
	60	12	0.016	12.3	4.39
	60	12	1.646	12.3	214.59
	60	12	1.364	12.3	158.06
Donnybrook	40	12	2.425	10.0	324.29
	40	12	2.868	10.0	409.17
	40	14	2.870	8.1	496.21

	40	14	3.563	8.1	680.01
	60	10	1.141	15.2	151.75
	60	10	1.467	15.2	205.90
	60	10	1.956	15.2	288.04
	60	10	2.445	15.2	346.54
	60	10	2.934	15.2	435.74
	60	12	1.986	12.3	281.49
	60	12	2.428	12.3	358.08
	60	12	2.869	12.3	441.99

(b)

Core	T **(°C)**	P **(MPa)**	u **(mm s^{-1})**	D **(10^{-8} m^2 s^{-1})**	K_{corr} **(10^{-8} m^2 s^{-1})**	Θ_m	β **(10^{-4} s^{-1})**
Ketton	40	8	0.018	16.4	10.48	1.000	-
	40	8	0.031	16.4	18.60	0.785	3.39
	40	8	0.053	16.4	17.08	0.707	6.16
	40	8	0.072	16.4	18.29	0.712	8.29
	40	10	0.006	12.5	6.39	1.000	-
	40	10	0.011	12.5	8.49	1.000	-
	40	10	0.028	12.5	15.59	1.000	-
	40	10	0.056	12.5	17.09	0.763	6.55
	40	10	0.086	12.5	18.62	0.753	9.58
	40	10	0.141	12.5	27.06	0.700	16.38
	40	10	0.224	12.5	44.14	0.718	24.05
	40	10	0.336	12.5	57.11	0.737	36.89
	40	10	0.561	12.5	99.73	0.758	59.84
	40	10	0.787	12.5	143.05	0.758	87.22
	40	10	1.124	12.5	212.49	0.764	124.55
	40	10	1.682	12.5	399.90	0.731	191.12
	40	12	1.743	10.0	381.70	0.791	187.02
	40	14	1.908	8.1	424.03	0.809	209.90
	40	14	2.323	8.1	538.10	0.813	260.90
	60	10	0.015	15.2	10.03	1.000	-
	60	10	0.277	15.2	39.73	0.794	28.20
	60	10	0.745	15.2	115.94	0.787	76.45
	60	10	1.192	15.2	217.73	0.785	122.66

Table 3. Dispersivities, α, in units of millimetres, determined by regression of Equation (2) to asymptotic Dispersion coefficients measured in this work and by Honari et al. (2013) using various constraints on the power law exponent, n. Exponents of $n = 1.2$ for sandstones and $n = 1.4$ for carbonates have been shown by simulations to better represent advective mixing behaviour in the limit of high Pe_m and were used to construct Figure 9(a).

α [mm]	**Berea**	**Donnybrook**	**Estaillades**	**Ketton**
***n* = 1**	0.37	1.43	1.2	1.59
***n* = 1.2**	0.36	0.85		
***n* = 1.4**			0.57	0.63